

# Data-driven classification of ventilated lung tissues using electrical impedance tomography

Camille Gómez-Laberge<sup>1</sup>, Matthew J. Hogan<sup>2</sup>, Gunnar Elke<sup>3</sup>,  
Norbert Weiler<sup>3</sup>, Inéz Frerichs<sup>3</sup> and Andy Adler<sup>4</sup>

<sup>1</sup> Department of Anesthesiology, Perioperative and Pain Medicine, Children's Hospital Boston, Harvard Medical School, Boston 02115, USA

<sup>2</sup> Neuroscience Program, Ottawa Hospital Research Institute, Ottawa K1H 8M5, Canada

<sup>3</sup> Anaesthesiology and Intensive Care Medicine, University Medical Centre Schleswig-Holstein, Campus Kiel, D-24105 Kiel, Germany

<sup>4</sup> Department of Systems and Computer Engineering, Carleton University, Ottawa K1S 5B6, Canada

E-mail: [Camille.Gomez@childrens.harvard.edu](mailto:Camille.Gomez@childrens.harvard.edu)

**Abstract.** Current methods for identifying ventilated lung regions utilizing electrical impedance tomography (EIT) images rely on dividing the image into arbitrary regions of interest (ROI), manually delineating ROI, or forming ROI with pixels whose signal properties surpass an arbitrary threshold. In this article, we propose a novel application of a data-driven classification method to identify ventilated lung ROI based on forming  $k$  clusters from pixels with correlated signals. A standard first-order model for lung mechanics is then applied to determine which ROI correspond to ventilated lung tissue. We applied the method in an experimental study of 16 mechanically ventilated swine in the supine position, which underwent changes in positive end-expiratory pressure (PEEP) and fraction of inspired oxygen ( $F_{I}O_2$ ). In each stage of the experimental protocol, the method performed best with  $k = 4$  and consistently identified 3 lung tissue ROI and 1 boundary tissue ROI in 15 of the 16 subjects. When testing for changes from baseline in lung position, tidal volume, and respiratory system compliance, we found that PEEP displaced the ventilated lung region dorsally by 2 cm, decreased tidal volume by 1.3%, and increased the respiratory system compliance time constant by 0.3 s.  $F_{I}O_2$  decreased tidal volume by 0.7%. All effects were tested at  $p < 0.05$  with  $n = 16$ . These findings suggest that the proposed ROI detection method is robust and sensitive to ventilation dynamics in the experimental setting.

*Keywords:* electrical impedance tomography, lung ventilation, pattern recognition, cluster analysis, acute lung injury.

## 1. Introduction

Electrical impedance tomography (EIT) can be utilized as a noninvasive lung ventilation imaging modality. EIT lung imaging shows promise as a valuable tool for the bedside

monitoring of mechanically-ventilated patients in the intensive care unit (ICU) (Wolf & Arnold 2006). In essence, EIT uses voltage and current stimulation patterns via a series of electrodes in order to apply and measure electrical energy along the chest circumference. These data are in turn used to determine changes in the regional conductivity distribution in the chest as a regularized inverse solution of the generalized Laplace equation (Adler et al. 2009). While improvements in the spatial resolution of EIT remain an important pursuit for clinical applications, the present spatiotemporal resolution and sensitivity to conductivity change have been shown to be sufficient for monitoring regional lung ventilation (Frerichs et al. 1999). Observational studies in clinic also suggest that EIT could play an important role in the treatment of lung disease, such as in acute lung injury (ALI) and acute respiratory distress syndrome (ARDS) (Victorino et al. 2004, Wolf & Arnold 2005).

The challenge of regionally monitoring lung ventilation in patients is formidable because, according to computed tomography (CT) studies, ALI-ARDS affects lung tissue heterogeneously (Gattinoni et al. 2006). Consequently, ventilated ICU patients exhibit a variety of collapsed (atelectatic), properly recruited, and overdistended lung regions (Wolf & Arnold 2006). This is compounded with the known gravitational effect that produces a dorsoventral gradient of alveolar recruitment in supine patients (Frerichs et al. 1996, Frerichs et al. 2003). However, the possibility of obtaining timely information on regional lung tissue state during mechanical ventilation would provide valuable insight on the regional effects of ventilation parameters for the development of EIT-guided ventilation protocols to maximize proper recruitment and minimize atelectasis and overdistension (Wolf & Arnold 2006). Indeed, recent clinical evidence shows that patients with ARDS will respond differently to the application of positive end-expiratory pressure (PEEP) depending on the potential recruitability of their lungs (Caironi et al. 2010). While lung recruitability is currently determined during an isolated CT scan, more information about the patient’s response could be obtained by continuously monitoring mechanical ventilation using EIT. In this setting, the automatic classification of lung tissues that respond distinctly during ventilation would be instrumental to study the regional effects of ventilation protocols and apply these observations to optimize them in a patient-specific and adaptive manner.

Currently, all proposed approaches to determining physiological parameters of ventilation from EIT data may be classified as “model-based” techniques. Such techniques fit data to a predefined set of specific parameters. They are effective in finding patterns fitting the specified model; however, these approaches would overlook potentially relevant patterns in the data which are distinct from the specified model. In this work, we are motivated by the potential utility of data-driven techniques, which do not require a particular model to be specified in order to search for structured patterns in the data. We envision a complementary role for data- and model-driven techniques: data-driven algorithms could help discover novel structure in exploratory studies, while model-based algorithms have an enhanced specificity to identify a particular structure in a clinical test.

Toward this goal, here we show how data-driven classification can be used to automatically distinguish distinct lung regions from EIT data based on tissue expiratory dynamics. The proposed approach is based on data-driven methods for functional brain imaging (Goutte et al. 1999, Jarmasz & Somorjai 2002, Gómez-Laberge et al. 2008, Gómez-Laberge et al. 2011) involving: i) fuzzy cluster analysis for the partitioning of EIT conductivity maps into regions with distinct conductivity dynamics, and ii) a lung tissue classification model-based on regional conductivity dynamics. In contrast to classical EIT analysis methods (Frerichs 2000), this approach does not require predefined regions of interest for analysis; e.g., partitioning the image using geometrical or regression models (Pulletz et al. 2006). Instead, the EIT data set is automatically partitioned into regions, each exhibiting distinct dynamics. The results demonstrate the classification of several lung regions having distinct temporal responses to ventilation for an appropriate choice of clusters. This study also provides evidence supporting i) the dorsoventral gradient of alveolar recruitment during ventilation in the supine body position, ii) the expected increase in respiratory system compliance when PEEP is applied, and iii) the decrease in variability of tidal volume with PEEP and elevated fraction of inspired oxygen ( $F_{I}O_2$ ). Furthermore, we introduce novel analytical perspectives for EIT data based on the stability of clusters during the variation of ventilation parameters and on the hierarchical progression of clusters for EIT analysis. These aspects are demonstrated here to show their utility for the exploration of ventilation responses in case studies.

## 2. Materials & Methods

The first section begins with a description of the animal lung ventilation model with detail of the pharmacological materials and the ventilation protocol. Next, the EIT instrumentation and materials are listed, and the data acquisition and image reconstruction methods are described. The second section presents the analysis methods used to classify ventilated lung regions. It begins with a pre-processing step to mitigate unrelated physiological noise. Next, the data-driven clustering algorithm *fuzzy k-means* is presented from an applied perspective. The section ends with a compliance model used to classify data clusters that represent ventilated lung tissue. The third section describes the approach used to compare results within the ventilation protocol and between subjects. A spatial measure of lung displacement and a temporal measure of respiratory system compliance and tidal volume are given.

### 2.1. Lung ventilation model and EIT imaging

A ventilation protocol inducing controlled changes in PEEP and  $F_{I}O_2$  was performed on sixteen anaesthetized pigs of mass  $39 \pm 4$  kg in supine position, referred to as subjects 1-16. The study took place at the University Medical Center of Schleswig-Holstein, Campus Kiel in Germany and was approved by the university committee for animal

care. The animals were first sedated with azaperon (8 mg/kg) and then anaesthetized by continuous intravenous infusion of propofol (6-12 mg/kg/h) and sufentanil (10  $\mu$ g/kg/h). Vecuronium bromide (0.1 mg/kg) was administered for muscle paralysis. Subsequently, the animals were intubated and connected to a ventilator (Siemens Servo 900 C, Siemens-Elma, Solna, Sweden). Hemodynamic and ventilatory parameters including heart rate, carbon dioxide partial pressure (PCO<sub>2</sub>) in respired gas, arterial oxygen saturation (S<sub>a</sub>O<sub>2</sub>), airway pressure and lung compliance were continuously monitored using the S/5 anaesthesia monitoring system with a gas-density compensated module (M-CAIOV, Datex Ohmeda, Helsinki, Finland). All animals were ventilated in a volume-controlled mode with constant tidal volume, respiratory rate (20 breaths/min), and inspiration-to-expiration ratio of 1:2 in order to maintain normocapnia (P<sub>end-tidal</sub>CO<sub>2</sub> 35-45 mmHg). Each animal underwent a ventilation protocol which began with a baseline state (15 min, PEEP 0 cmH<sub>2</sub>O, 0.21 F<sub>I</sub>O<sub>2</sub>) followed by a PEEP state (5 min, PEEP 5-10 cmH<sub>2</sub>O, 0.21 F<sub>I</sub>O<sub>2</sub>), an elevated F<sub>I</sub>O<sub>2</sub> state (15 min, PEEP 0 cmH<sub>2</sub>O, 1.0 F<sub>I</sub>O<sub>2</sub>), and a return-to-baseline state (15 min). Subjects 1-8 underwent PEEP at 5 cmH<sub>2</sub>O PEEP and subjects 9-16 at 10 cmH<sub>2</sub>O.

EIT data were acquired (Goe-MF II, Cardinal Health, Höchberg, Germany) with sixteen Ag/AgCl electrodes (Blue Sensor BR-50-K, Ambu, Bad Nauheim, Germany) that were evenly spaced around the chest circumference on the transverse plane at the level of the sixth intercostal space. Electrical current (50 kHz, 5 mA rms) was injected between all adjacent pairs of electrodes, while the remaining electrodes measured the voltage with respect to a distal reference electrode, yielding one *frame*. During each ventilation state of the protocol, 780 frames were acquired over one minute (13 frames/s). Thus, for each animal, a one-minute EIT session was performed during each of the four, 15-minute ventilation states of the protocol. The starting point of the EIT scan was chosen on the final minute of each ventilation state in order to allow time for the respiratory system to transition from the previous settings to the new settings. Image reconstruction of the internal conductivity distribution was computed using a one-step linearized Gauss-Newton estimate using a regularization penalty term based on a Laplacian filter with hyperparameter value corresponding to a noise figure of 0.60 (Adler & Guardo 1996). These reconstructions were implemented in EIDORS (version 3.3) (Adler & Lionheart 2006) and produce *normalized difference EIT* data, which measure conductivity change as  $\Delta\sigma = (\sigma - \sigma_r)/\sigma_r$ , i.e., the fractional conductivity change from a reference measurement  $\sigma_r$  (Adler et al. 2009). All conductivity data in this work are presented as normalized conductivity  $\Delta\sigma$ .

## 2.2. Data-driven EIT tissue classification

The EIT session is a time series for each image pixel of one-minute duration. Approximately twenty breaths take place during the one-minute session. To mitigate breath asynchronous signals (e.g., uncorrelated motion, heartbeat) a breath-averaged EIT time series is produced. It represents the average conductivity change taking place

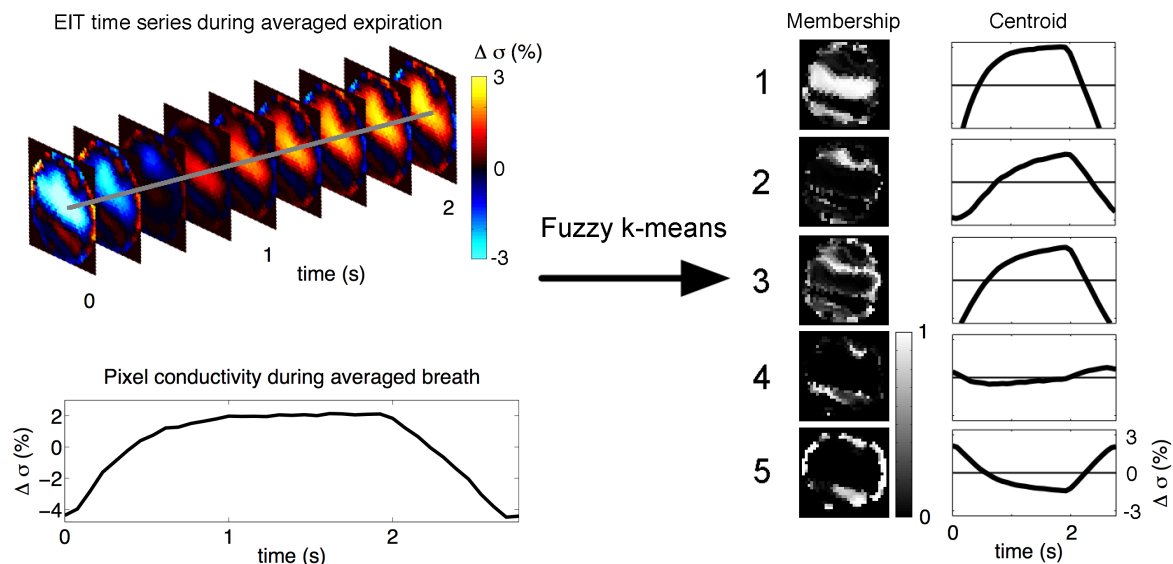


**Figure 1.** Lung tissue classification method overview. The breath-averaged EIT time series shows the progressive conductivity change during expiration (*top left*). The pixel conductivity ( $\Delta\sigma$ ) corresponding to the grey line through the EIT data is plotted for the entire averaged-breath (*bottom left*), where time is on the abscissa and conductivity is on the ordinate. The EIT data are clustered by the fuzzy  $k$ -means algorithm for  $k = 5$  producing the membership maps in grayscale and centroids shown (*right*), where time is on the abscissa and conductivity is on the ordinate. Data shown are from subject 1 at baseline.

in each pixel during a breath and is obtained as follows. First, a global time series signal  $\boldsymbol{\mu}$  is computed, such that, at every time point  $t$  throughout the session,  $\boldsymbol{\mu}[t]$  is the average of all pixel conductivity values. Then, the signal  $\boldsymbol{\mu}$  finding the local minima corresponding to the maximally inflated lungs. The first and last partial breaths in the session are discarded, and the remaining breaths are ensemble-averaged over the shortest breath interval. We express the breath-averaged EIT time series as  $\mathbf{z} = \mathbf{z}[x, t]$  for pixel index  $x \in \mathbb{N}^2$  at time  $t$ . All subsequent analyses described in this article pertain to  $\mathbf{z}[x, t]$  computed for each part of the experimental paradigm.

All sessions in this study have 19-21 breaths of 2.77-2.92 s duration with the exception of one session (subject 10) that ran for only 30 seconds and collected 10 breaths. All breath-averaged sessions have 36-38 time points  $N_t$  and  $N_x = 32^2$  pixels arranged along the left-right (horizontal) and dorsoventral (vertical) axes. A representative session (subject 1, baseline) is shown on the left side of Fig. 1. An increase in conductivity during expiration is seen in this session. The conductivity in the pixel indicated by the grey line through the time series is plotted for the entire breath ( $\sim 2$  s expiration followed by  $\sim 1$  s inspiration).

A data-driven approach is used to partition the pixels from  $\mathbf{z}$  into  $k$  clusters with the objective that the best correlated pixel time series are in the same cluster. Hence, the

tissue contributing to each pixel may be classified based on its conductivity during the ventilation protocol. The algorithm is called *fuzzy k-means* developed by (Dunn 1973) and is based on the fuzzy set theory of (Zadeh 1965). The clusters in the solution assign a membership, a real number  $0 \leq u \leq 1$ , to each pixel  $x$  according to a correlation-based metric  $d$  that measures the distance between the pixel time series  $\mathbf{z}[x]$  and the average time series of the cluster of pixels  $\mathbf{v}_i$ , called the *cluster centroid* (Dunn 1973). The metric is called the *hyperbolic correlation distance* (Golay et al. 1998) and depends only on the phase difference between time series

$$d(\mathbf{z}[x], \mathbf{v}_i) = \sqrt{\frac{1 - r(\mathbf{z}[x], \mathbf{v}_i)}{1 + r(\mathbf{z}[x], \mathbf{v}_i)}}, \quad (1)$$

where  $r(\cdot, \cdot)$  is the Pearson product-moment correlation.

The memberships satisfying the solution form a  $k \times N_x$  matrix  $\mathbf{U} = [\mathbf{u}_1, \dots, \mathbf{u}_k]^\top$ , where each vector contains the memberships for all pixels in  $\mathbf{z}$ . The corresponding centroids form a  $k \times N_t$  matrix  $\mathbf{V} = [\mathbf{v}_1, \dots, \mathbf{v}_k]^\top$ , where each vector is the membership-weighted average of all time series in  $\mathbf{z}$ . The right side of Fig. 1 shows the solution of the illustrated session for  $k = 5$ . Here, the membership vectors are mapped onto the image with a grey intensity scale, and the centroid vectors are plotted as conductivity change versus time. Technically, each time series  $\mathbf{z}[x, t]$  for  $t = 1, \dots, N_t$  is mapped to a point in the metric space  $(\mathbb{R}^{N_t}, d)$ . Given  $k$  and an initial partition  $\mathbf{U}_0$ , the algorithm minimizes the least squares objective function

$$J(\mathbf{U}, \mathbf{V}, \mathbf{z}) = \sum_{i=1}^k \sum_{j=1}^{N_x} u_i^2[x_j] d^2(\mathbf{z}[x_j], \mathbf{v}_i), \quad (2)$$

where  $d(\cdot, \cdot)$  is a distance function described below. Equation (2) is minimized by iterating between the centroid computation

$$\mathbf{v}_i = \frac{\sum_{j=1}^{N_x} u_i^2[x_j] x_j}{\sum_{j=1}^{N_x} u_i^2[x_j]}, \quad \text{for } i = 1, \dots, k \quad (3)$$

and the membership computation for each pixel  $x$

$$\mathbf{u}_i[x] = \frac{d^{-2}(\mathbf{z}[x], \mathbf{v}_i)}{\sum_{j=1}^k d^{-2}(\mathbf{z}[x], \mathbf{v}_j)}, \quad \text{for } i = 1, \dots, k. \quad (4)$$

The stopping criterion requires that the maximum Euclidean distance between iterations of  $\mathbf{V}$  be smaller than  $\epsilon = \|\boldsymbol{\mu}\|/1000$ . That is, the centroid vectors must not move in  $\mathbb{R}^{N_t}$  by more than one thousandth of the magnitude of the global time series vector.

In order to compare clusters between protocol ventilation states and between sessions, a fixed number of clusters was chosen that produces *stable partitions* for the largest number of sessions. Fig. 2 illustrates our idea of a stable partition during a

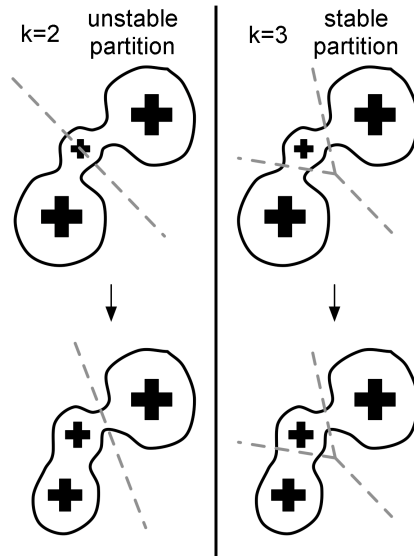


**Figure 2.** Partition stability during state changes. A fictitious data set undergoing a state change (direction of arrow) is partitioned with  $k = 2$  (left) and  $k = 3$  (right). In the space  $(\mathbb{R}^N, d)$ , the data points are scattered within a boundary (solid line) and are most concentrated near three foci (crosses). The state change causes a migration of points from one focus to another. The unstable 2-partition shifts considerably during the change, while the stable 3-partition remains in place.

state change. In the metric space, the data form three foci of data points. A 2-partition (left panel) is unstable after the state change due to a migration of points from one focus to another, while the 3-partition (right panel) is not disturbed by the state change. The inter-state comparison of each cluster is accomplished by corresponding the memberships  $\mathbf{U}$  from all ventilation states back to the baseline state. This is done by choosing the bijective correspondence between ventilation states that maximizes the inner product between membership vectors. For each baseline vector  $\mathbf{u}_{B,i}$ , only one vector from the PEEP state will correspond to  $\mathbf{u}_{B,i}$  because its inner product  $\langle \mathbf{u}_{PEEP,j} | \mathbf{u}_{B,i} \rangle = \sqrt{\sum_x \mathbf{u}_{PEEP,j}[x] \mathbf{u}_{B,i}[x]}$  is largest from that state. The same process is repeated for the elevated  $F_{I}O_2$  and return-to-baseline ventilation states. Considerable inconsistencies of the inner product between ventilation states are used to detect unstable partitions.

In each session, the clusters that represent ventilated lung tissue are classified by fitting the expiration part of each centroid to a first order model

$$\Delta\sigma = A + B(1 - e^{-t/\tau}), \quad (5)$$

where the time constant  $\tau > 0$  is in seconds, and  $A < 0$  and  $B > 0$  are conductivity offset and scale parameters, respectively. In equation (5),  $\Delta\sigma$  satisfies the step-response signal for a circuit composed of a resistance element in series with a compliance element; this model has been shown to be valid for lung mechanics during tidal breathing (Webster 1998). In this model, the parameter  $\tau$  is proportional to the product of airway resistance and respiratory system compliance. According to the literature, we expect

that changes in PEEP will primarily affect respiratory system compliance by distending the parenchyma, and that changes in  $F_{I}O_2$  may have an opposite effect on by causing absorption atelectasis (Rothen et al. 1995). Therefore, we hypothesized that changes in respiratory system compliance between these ventilation states can be detected by proportional changes in  $\tau$ .

For example, only clusters 1-3 in Fig. 1 fit this model. Equation (5) is fit to the data using a multivariate unconstrained nonlinear minimisation (Lagarias et al. 1998) of the residual sum of squares. The initial parameters used are  $\tau = 1$  s,  $A = -0.1$ , and  $B = 0.3$ ; the residual error tolerance is  $10^{-4}$ . Clusters that fit the model are classified as containing lung tissue and are subsequently included in the inter-session analysis.

### 2.3. Plethysmographic surrogate measures using EIT

The effects of PEEP and elevated  $F_{I}O_2$  are investigated by analysing the conductivity changes in lung tissue, which are used as measures of i) the displacement of lung ventilation distribution (we use the term ‘‘lung displacement’’ for brevity), and ii) expiratory dynamics between ventilation states. Although each centroid provides a good representation of the dynamics in a cluster, they should not be used for parameter estimation of the underlying data  $\mathbf{z}$ . This is evident by observing that in (3), the centroid  $\mathbf{v}_i$  differs from the membership-weighted average of the data by a multiplicative constant. Consequently, for parameter estimation of the data, we use  $\mathbf{U}$  to compute the membership-weighted averages  $\tilde{\mathbf{v}}_i = \sum_x \mathbf{z}[x] \mathbf{u}_i[x] / \sum_x \mathbf{u}_i[x]$ . Moreover, the fuzzy  $k$ -means algorithm adjusts  $\mathbf{U}$  and  $\mathbf{V}$  simultaneously to converge to the optimal  $k$ -partition in the least squares sense. Thus, to avoid the redundancy of inter-state changes in  $\tilde{\mathbf{v}}_i$  resulting merely from changes in  $\mathbf{u}_i$ , the lung displacement analysis is performed while fixing  $\tilde{\mathbf{v}}_i$  across ventilation states, and in turn, the dynamical analysis is done with  $\mathbf{u}_i$  fixed.

Inter-state estimates of lung displacement are performed by calculating the centre of mass  $\bar{x}$  for each lung tissue cluster. The baseline  $\tilde{\mathbf{v}}_{B,i}$  of these clusters are correlated with all pixel time series for each state to produce a correlation map  $\mathbf{r}[x] > \theta$  for a preset threshold  $\theta$ . For each  $\tilde{\mathbf{v}}_i$ -fixed cluster, the displacement of  $\bar{x}$  is computed across all ventilation states. Inter-state estimates of respiratory system compliance and tidal volume are performed by fitting (5) to  $\tilde{\mathbf{v}}_i$  of each lung tissue cluster. For these baseline clusters, the membership-weighted averages  $\tilde{\mathbf{v}}_i$  compute the model parameters of (5) across all ventilation states. Data from each ventilation state are compared to ‘Baseline I’ using a two-tailed paired  $t$ -test with a type I error rate of  $\alpha = 0.05$ .

## 3. Results

For each subject, EIT images were reconstructed for each ventilation state and were analyzed using the proposed algorithm as follows: i) fuzzy cluster analysis to partition EIT images into distinct regions, ii) lung tissue classification based on regional image

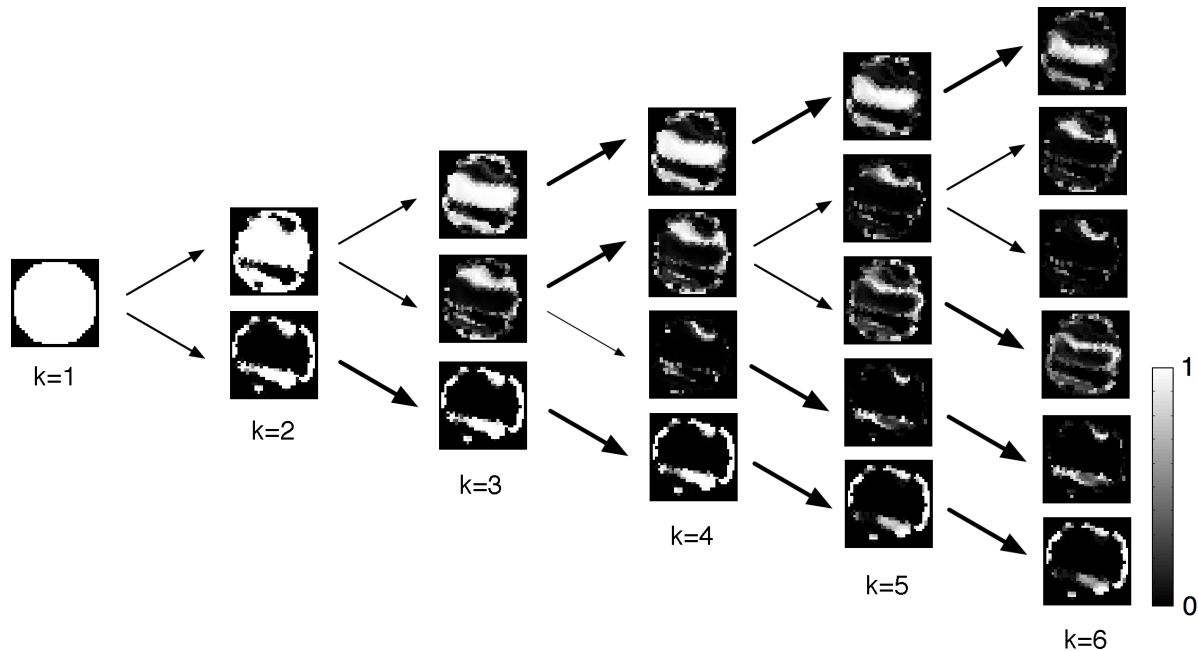


**Figure 3.** Hierarchical progression of fuzzy  $k$ -means clustering. The membership maps in grayscale from the data set in figure 1 (subject 1 at baseline) are presented for  $k = 1, \dots, 6$ . The clusters between subsequent partitions form a hierarchical progression demonstrating the consistency of the algorithm applied to these data. The thickness of the arrows indicates the similarity between clusters in subsequent partitions.

dynamics, and iii) the estimation of standard ventilation parameters from EIT data.

### 3.1. Hierarchical progression of the $k$ -partitions

The consistency of the algorithm is verified by examining the relationship between subsequent  $k$ -partitions for increasing  $k$ . As we intuitively expect, the clusters with largest variance in the  $k$ -partition are further subdivided in the  $(k+1)$ -partition, and the remaining clusters stay relatively unchanged. This hierarchical progression is shown in Fig. 3, using the same data set from Fig. 1 (subject 1 at baseline), where the membership maps are shown for  $k = 1, \dots, 6$ . The arrows illustrate the relationship between  $k$  and  $k+1$  partitions; the thickness of each arrow qualitatively describes the similarity between the clusters. At  $k = 2$ , the boundary cluster first appears (bottom cluster) and remains intact afterward. This boundary signal is the well known consequence of chest wall expansion and contraction during breathing (Adler et al. 1996). Next, at  $k = 3$ , the main contribution from the lungs appears (top cluster); the middle cluster in  $k = 3$  progressively splits until  $k = 6$ . This hierarchical behaviour was seen for all 64 data sets used in this study (not shown) and demonstrates the consistency of the algorithm.

### 3.2. Partition stability during ventilation protocol

The order in which the regions subdivide as  $k$  grows is informative of the heterogeneity of the data set. Typically, incrementing  $k$  leads to the splitting of only one cluster; i.e., the one with the largest variance. Finally, we also observe that the average membership value of each cluster decreases as  $k$  grows. Figure 3 also illustrates this effect as the number of dark grey pixels in each cluster increases with  $k$ . These observations led us to avoid seeking a single value for  $k$  but instead to use a general approach that also considers how  $k$  affects the stability of the partitions throughout the ventilation protocol for each session.

In this 16-subject study,  $k = 4$  yields fifteen subjects with stable partitions throughout the baseline, PEEP,  $F_{I}O_2$ , and return-to-baseline ventilation states. These partitions consistently identify one boundary region and three distinct lung regions stratified in the dorsoventral direction throughout the ventilation protocol. Subject 12 contains unstable 4-partitions at PEEP,  $F_{I}O_2$ , and return-to-baseline. At  $k = 5$ , seven sessions have stable partitions that identify the regions described and an additional cluster with an attenuated ventilation response which involves the ventral area near the heart. These regions, however, are not as consistently clustered as for  $k = 4$ . Figure 4 illustrates a stable 5-partition (subject 1) throughout the ventilation protocol, where clusters 1-3 fit the compliance model. The remaining nine subjects have unstable 5-partitions and, interestingly, seven of them have instabilities only occurring during PEEP. Figure 5 demonstrates one of these seven cases (subject 14) where the partition becomes unstable during PEEP and is subsequently restored. Lung region cluster 3 is split (green lines), and boundary clusters 4 and 5 are merged (blue lines) only during PEEP and are restored afterward. The two remaining unstable subjects are 11 and 12, having instabilities during  $F_{I}O_2$  and return-to-baseline, respectively. Analysis at  $k = 6$  yields five stable subjects and nine PEEP, one  $F_{I}O_2$ , and one return-to-baseline unstable subjects. A strong cardiac artifact is also present in five of the subjects, regardless of the  $k$  value used. For example, Fig. 5 also shows a 2 Hz frequency artifact (red box), which matches the heart rate of 128 bpm (2.1 Hz) recorded at the time of acquisition.

### 3.3. Lung displacement, compliance, and tidal volume

EIT-based measures of lung displacement, compliance, and tidal volume are estimated using the results from  $k = 4$ , which yields eleven subjects with stable partitions and without cardiac artifact. For each subject, the clusters that fit the compliance model (5) are selected for the parameter estimation. In this case, 3 clusters per session were selected, yielding 33 measurements for parameter estimation for each state. In a preliminary approach, we overestimate the standard error of the mean (SEM) by dividing the standard deviation of the 33 measurements by  $\sqrt{11}$ .

Summary results are shown in Fig. 6(a) for the centre of mass as a fractional distance from the image centre relative to the thoracic diameter, in Fig. 6(b) for the compliance model scaling parameter  $B$  in conductivity units  $\Delta\sigma$ , and in Fig. 6(c) for the compliance

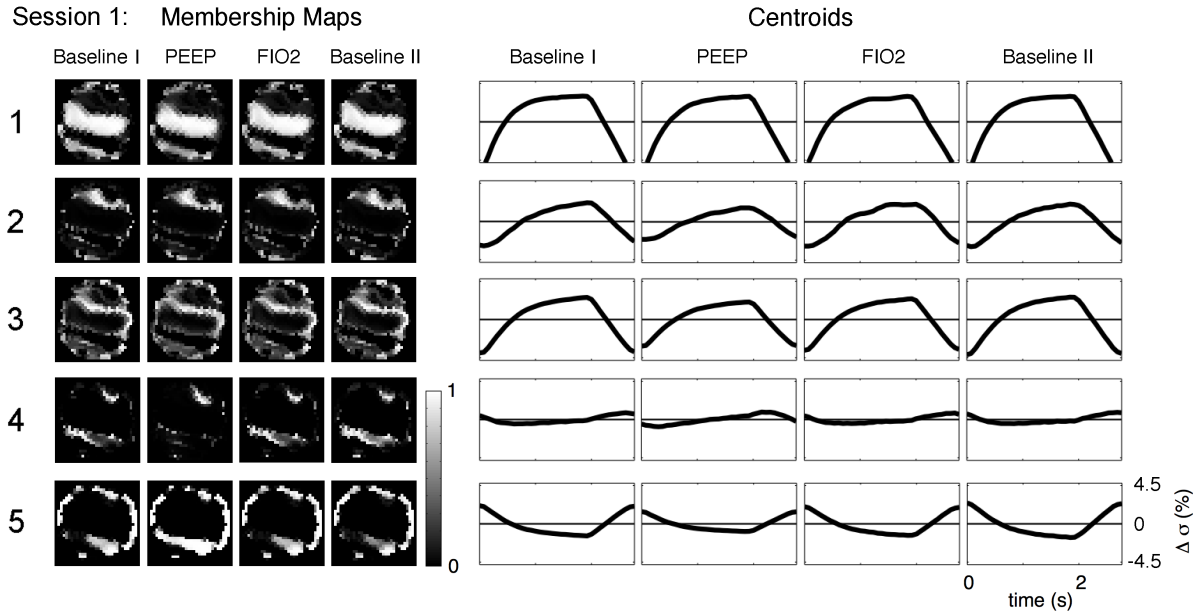


**Figure 4.** Stable 5-partition throughout the ventilation protocol. Solution from subject 1 demonstrates a stable partition as was observed in 7 of 16 subjects. Columns represent the  $k = 5$  membership maps in grayscale (*left*) for all ventilation states arranged in rows. The corresponding cluster centroids are shown in the same configuration (*right*), where time is on the abscissa and conductivity is on the ordinate. The boundary cluster 5 and clusters 1-3 containing lung tissue are consistently found. Cluster 4, however, varies between cases, exhibiting an attenuated compliance or boundary movement signal.

model time constant  $\tau$  in seconds. These represent changes between ventilation states of lung position, tidal volume, and respiratory system compliance, respectively. For the centre of mass estimates, we pre-selected a threshold value of  $\theta = 0.97$  for all subjects based on a visual check to ensure the resulting correlation maps reasonably represent the membership maps obtained during cluster analysis.

These results suggest that PEEP and  $F_{I}O_2$  have appreciable effects on EIT data. In none of the graphs, however, is the Baseline II state significantly different from the Baseline I. There is a significant lung displacement in the dorsal direction by 1% of the thoracic diameter (2 cm) when PEEP is applied ( $p < 0.05$ ). The estimated time constant during expiration increases significantly ( $p < 0.05$ ) by 0.3 seconds when PEEP is applied. Finally, the tidal volume estimates decrease significantly ( $p < 0.05$ ) during PEEP and  $F_{I}O_2$  by 1.3% and 0.7%, respectively.

#### 4. Discussion

In this article, a novel data-driven EIT approach to classify lung tissue based on their expiratory dynamics is proposed. We demonstrate how such information could be used to monitor how these distinctly-behaving tissues evolve during ventilation

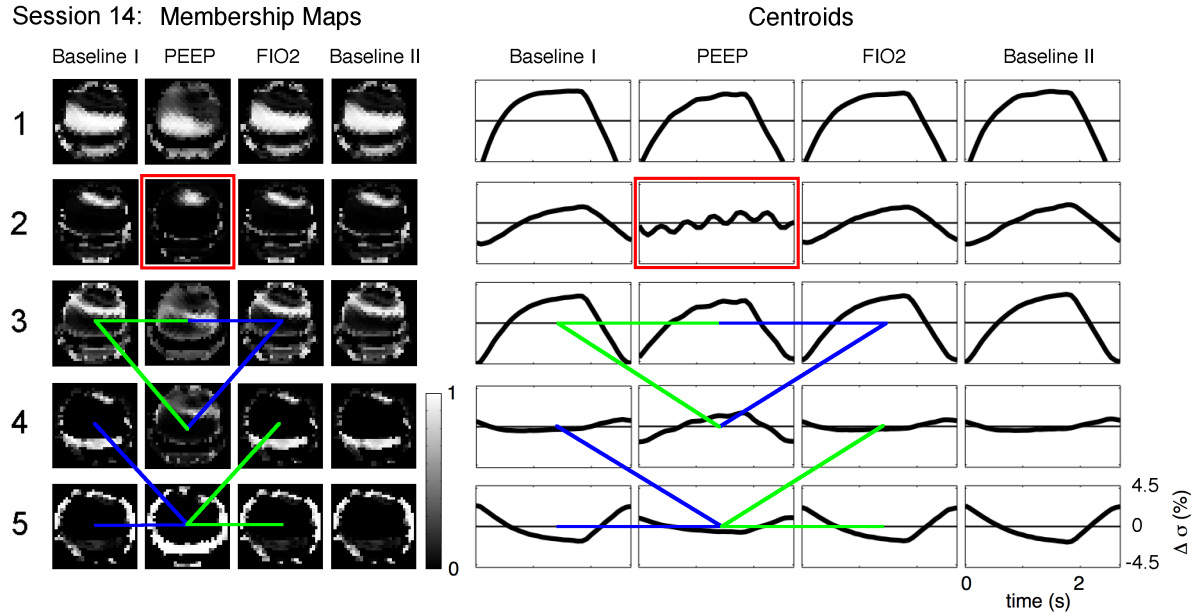


**Figure 5.** Unstable 5-partition during PEEP. Solution from subject 14 demonstrates an unstable partition as was observed in 9 of the 16 subjects. Columns represent the  $k = 5$  membership maps in grayscale (*left*) for all ventilation states arranged in rows. The corresponding cluster centroids are shown in the same configuration (*right*), where time is on the abscissa and conductivity is on the ordinate. During PEEP, lung region cluster 3 is split (green lines) and subsequently merged (blue lines), while the opposite occurs for boundary clusters 4 and 5. Also, a cardiac artifact (red box) is seen during PEEP.

protocol adjustments. The preliminary results shown here are encouraging because they not only corroborate the known effects of PEEP but also demonstrate how heterogeneously ventilated tissue can be identified and monitored. Namely, these data corroborate the known dorsoventral gradient of alveolar recruitment during supine ventilation, the expected increase in respiratory system compliance during PEEP application, and the decrease in tidal volume during ventilation with PEEP (Adler et al. 1996, Frerichs et al. 1996, Frerichs et al. 1999, Frerichs 2000, Wolf & Arnold 2005, Wolf & Arnold 2006, Wolf & Arnold 2007, Meier et al. 2008). Interestingly, our analysis did not reveal indications of atelectasis during the 15 minute protocol for 1.0  $F_{I}O_2$ , despite its detection in previous studies using computed tomography during comparable hyperoxic exposure in healthy (Brismar et al. 1985, Rothen et al. 1995) and injured lungs (Neumann et al. 1998). In line with evidence suggesting that respiratory system compliance is independent of atelectasis (Rothen et al. 1995), we conclude based on our findings that the surrogate measures of respiratory system compliance proposed here are also unaffected by the  $F_{I}O_2$ . Therefore, while the proposed measurements are sensitive to PEEP, and potentially PEEP-induced overdistension, complementary measures are likely required to indicate the presence of elevated  $F_{I}O_2$ -induced atelectasis.

This study is of course not without limitations. Regarding the proposed methods,

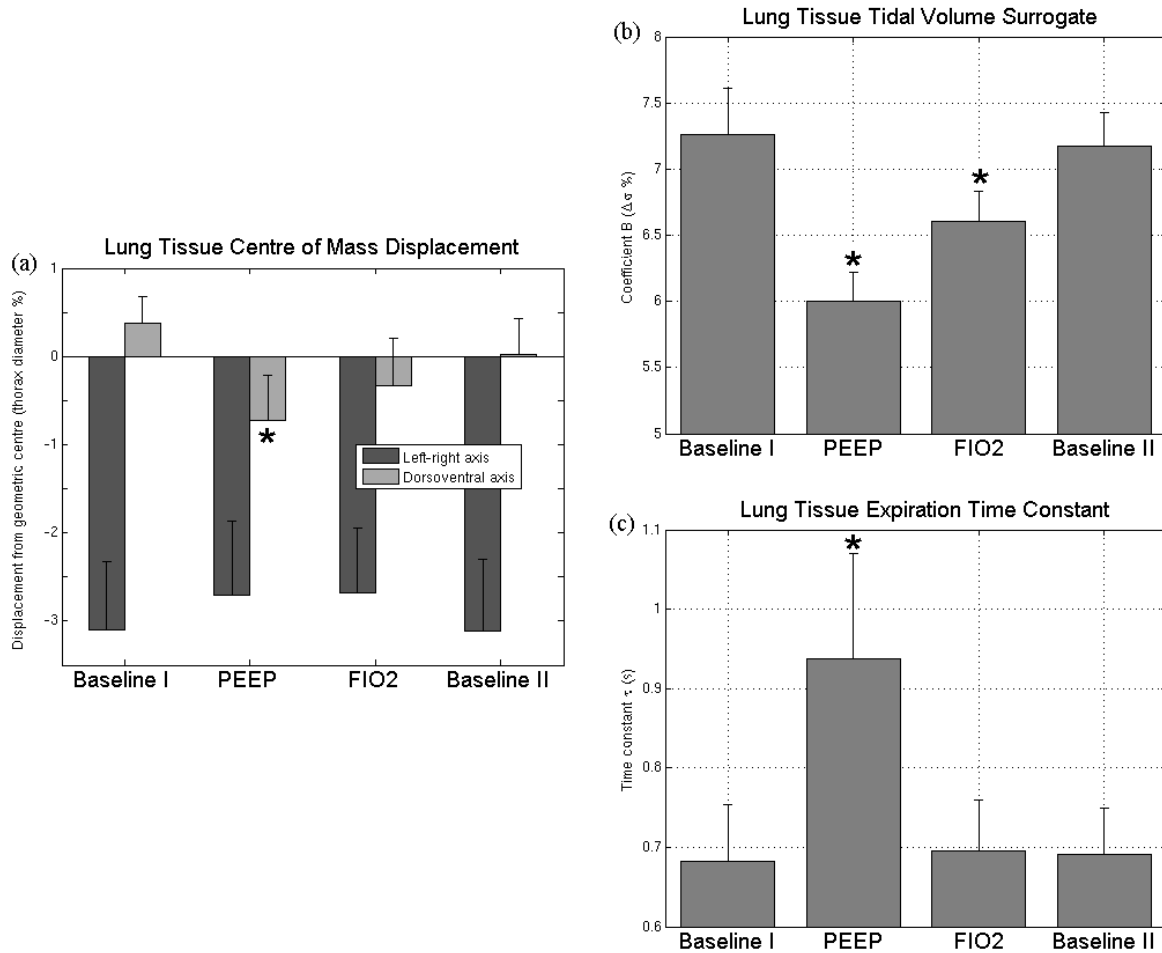


**Figure 6.** Estimates of changes in lung position, tidal volume, and respiratory system compliance between ventilation states. (a), Lung displacement is represented by the centre of mass coordinates shown as a fractional distance from the image centre relative to the thoracic diameter. (b), Tidal volume is represented by the compliance model scaling parameter  $B$  in conductivity units  $\Delta\sigma$ . (c), Respiratory system compliance is represented by the compliance model time constant  $\tau$  in seconds. Parameter estimates for each ventilation state were obtained from eleven sessions. Histograms represent the sample mean and its standard error. A ventilation state whose mean differs significantly from Baseline I is marked with an asterisk (two-tailed paired  $t$ -test with  $\alpha = 0.05$ ).

the algorithm stability and hierarchical progression used here to determine optimal  $k$  values were qualitatively assessed. This could be improved using a quantitative approach to determine inter-partition relationship, e.g., based on an inner product metric between membership map vectors. Regarding the mechanical model, we utilized the parameter  $\tau$  to detect changes in respiratory system compliance between ventilation states where PEEP and  $F_{I}O_2$  were varied. We do not rule out the possibility that concurrent changes in airway resistance also influenced the changes in  $\tau$ . Studies seeking to quantify changes between treatments in either resistance or compliance (but not both) must

keep the other variable fixed. Finally, the stages of our experimental protocol were not randomized; therefore, the unequivocal determination of the effect of ventilation states on EIT data cannot be established here. In particular, we cannot conclude on the effects observed during  $F_{I}O_2$ , since they may be confounded with those of the preceding PEEP maneuver. However, the initial baseline and return-to-baseline measurements were consistent throughout the study.

Acquiring continuous lung images during mechanical ventilation that reveal the proportion of atelectatic, recruited and overdistended tissue is of great value, since it would provide new insight into how atelectasis and overdistension evolve during ventilation and also how they relate to ICU patient outcome (Wolf & Arnold 2006). Furthermore, such a technique would play a key role in developing protocols that interactively maximise tissue recruitment while minimising ventilator-associated lung injury.

In conclusion, the preliminary results presented here show how data-driven EIT lung tissue classification is sensitive to the ventilatory dynamics of lung tissue. Our findings suggest that data-driven EIT lung tissue classification is robust in an experimental setting and may be useful to continually monitor regional lung injury at the bedside during mechanical ventilation. Such findings would represent a significant step toward the classification of the atelectasis, recruitment and overdistension of tissues affected by ALI and ARDS.

## Acknowledgments

This work was supported by the Natural Sciences and Engineering Council of Canada and the Heart and Stroke Foundation Centre for Stroke Recovery.

## References

- Adler A, Arnold J H, Bayford R, Borsic A, Brown B, Dixon P, Faes T J C, Frerichs I, Gangon H, Gärber Y, Grychtol B, Hahn G, Lionheart W R B, Malik A, Patterson R P, Stocks J, Tizzard A, Weiler N & Wolf G K 2009 *Physiol. Meas.* **30**, S35–S55.
- Adler A & Guardo R 1996 *IEEE Trans. Biomed. Eng.* **15**(2), 170–179.
- Adler A, Guardo R & Berthiaume Y 1996 *IEEE Trans Med Imaging* **43**(4), 414–420.
- Adler A & Lionheart W R B 2006 *Physiol. Meas.* **27**, S25–S42.
- Brismar B, Hedenstierna G, Lindquist H, Strandberg A, Svensson L & Tokics L 1985 *Anesthesiology* **62**, 422–428.
- Caironi P, Cressoni M, Chiumello D, Ranieri M, Quintel M, Russo S G, Cornejo R, Bugeo G, Carlesso E, Russo R, Caspani L & Gattinoni L 2010 *Am. J. Respir. Crit. Care Med.* **181**, 578–586.
- Dunn J 1973 *J. Cybern* **3**, 32–57.
- Frerichs I 2000 *Physiol. Meas.* **21**, R1–R21.
- Frerichs I, Dargaville P A, Dudykevych T & Rimensberger P C 2003 *Intensive Care Med.* **29**, 2312–2316.
- Frerichs I, Hahn G & Hellige G 1996 *Physiol. Meas.* **17**, A149–A157.
- Frerichs I, Hahn G, Schiffmann H, Berger C & Hellige G 1999 *Ann. NY Acad. Sci.* **873**, 493–505.
- Gattinoni L, Caironi P, Cressoni M, Chiumello D, Ranieri V M, Quintel M, Russo S, Patroniti N, Cornejo R & Bugeo G 2006 *N. Engl. J. Med.* **354**, 1775–1786.

- Golay X, Kollias S, Stoll G, Meier D, Valavanis A & Boesiger P 1998 *Magn. Reson. Med.* **40**, 249–260.
- Gómez-Laberge C, Adler A, Cameron I, Nguyen T & Hogan M J 2008 *IEEE Trans. Biomed. Eng.* **55**(10), 2372–2380.
- Gómez-Laberge C, Adler A, Cameron I, Nguyen T & Hogan M J 2011 *IEEE Trans. Biomed. Eng.* . In Press.
- Goutte C, Toft P, Rostrup E, Nielsen F A, & Hansen L K 1999 *NeuroImage* **9**, 298–310.
- Jarmasz M & Somorjai R L 2002 *Artif. Intell. Med.* **25**, 45–67.
- Lagarias J C, Reeds J A, Wright M H & Wright P E 1998 *SIAM J. Optim* **9**(1), 112–147.
- Meier T, Luepschen H, Karsten J, Leibbecke T, Großherr M, Gehring H & Leonhardt S 2008 *Intensive Care Med.* **34**(3), 543–550.
- Neumann P, Berglund J E, Mondéjar E F, Magnusson A & Hedenstierna G 1998 *Am. J. Respir. Crit. Care Med.* **158**, 1636–1643.
- Pulletz S, van Genderingen H R, Schmitz G, Zick G, Schädler D, Scholz J, Weiler N & Frerichs I 2006 *Physiol. Meas.* **27**, S115–S127.
- Rothen H U, Sporre B, Engberg G, Wegenius B, Högman M & Hedenstierna G 1995 *Anesthesiology* **82**, 832–842.
- Victorino J A, Borges J B, Okamoto V N, Matos G F J, Tucci M R, Carames M P R, Tanaka H, Sipmann F S, Santos D C B, Barbas C S V, Carvalho C R R & Amato M B P 2004 *Am. J. Respir. Crit. Care Med.* **169**, 791–800.
- Webster J G 1998 3 edn John Wiley & Sons, Inc. New York, USA chapter 9, pp. 375–380.
- Wolf G K & Arnold J H 2005 *Crit. Care Med.* **33**, S163–S169.
- Wolf G K & Arnold J H 2006 *Intensive Care Med.* **32**, 1290–1292.
- Wolf G K & Arnold J H 2007 *Crit. Care Med.* **35**, 1972–1978.
- Zadeh L 1965 *Inform. and Control* **8**(3), 338–353.